Optical Engineering

OpticalEngineering.SPIEDigitalLibrary.org

Reconstruction of the wavefront aberration from real interferometric data using a hybrid evolutionary optimization algorithm with Zernike polynomials

Juan Jaime Sánchez-Escobar
Liliana Ibeth Barbosa Santillán

SPIE.

Reconstruction of the wavefront aberration from real interferometric data using a hybrid evolutionary optimization algorithm with Zernike polynomials

Juan Jaime Sánchez-Escobar[a,*] **and Liliana Ibeth Barbosa Santillán**[b]
[a]Centro de Enseñanza Técnica Industrial, Nueva Escocia 1885, Fraccionamiento Providencia 5a Sección, C.P. 44638, Guadalajara, Jalisco, México
[b]Universidad de Guadalajara, CUCEA-Departamento de Sistemas de Información, Periférico Norte No. 799, Núcleo Universitario Los Belenes, C.P. 45100, Zapopan, Jalisco, México

Abstract. This paper describes the use of a hybrid evolutionary optimization algorithm (HEOA) for computing the wavefront aberration from real interferometric data. By finding the near-optimal solution to an optimization problem, this algorithm calculates the Zernike polynomial expansion coefficients from a Fizeau interferogram, showing the validity for the reconstruction of the wavefront aberration. The proposed HEOA incorporates the advantages of both a multimember evolution strategy and locally weighted linear regression in order to minimize an objective function while avoiding premature convergence to a local minimum. The numerical results demonstrate that our HEOA is robust for analyzing real interferograms degraded by noise. [DOI: 10.1117/1.OE.54.9.094102]

Keywords: interferometry; optical metrology; wavefront aberration; Zernike polynomials; numerical reconstruction; stochastic optimization; hybrid evolutionary optimization algorithms; inverse problems.

Paper 150384 received Mar. 24, 2015; accepted for publication Aug. 3, 2015; published online Sep. 10, 2015.

1 Introduction

Optical interferometry continues to be a major tool for determining the quality of the wavefront produced by an optical component.[1,2] The main advantages of diagnostic tests based on optical interferometry are their high precision and accuracy.[3]

A two-wave interferometer generates an interferogram by superimposing two wavefronts, one of which is, in general, either a plane or a spherical wavefront, while the other corresponds to an unknown wavefront whose shape is to be measured.[1,2,4] Hence, the difference between these wavefronts is defined as either optical path difference (OPD) or wavefront aberration.[5]

The problem of computing the wavefront aberration from an interferogram in terms of Zernike polynomials has been addressed by using the classical Gram-Schmidt method and the least-squares method.[6] While accurate modeling of the wavefront aberration with Zernike polynomials involves selecting the order of the polynomial expansion based on a list of the digitized fringe centers with their assigned order numbers,[7–10] this work describes a hybrid evolutionary optimization algorithm (HEOA) which automatically performs an accurate reconstruction of the wavefront aberration from a real interferogram once an objective function that depends on the Euclidean distance between the synthetic interferogram optimized in terms of the computed Zernike polynomials expansion coefficients and the analyzed real interferogram has been minimized while avoiding a local minimum. To prevent premature convergence to a local minimum, the proposed HEOA incorporates the advantages of both a multimember evolution strategy (MMES) and locally weighted linear regression (LWLR).

The MMES belongs to a class of optimization techniques called evolutionary algorithms, which are inspired by the principles of biological evolution. With an MMES, the optimization starts with a set of individuals, where each individual represents a real-valued vector that represents a candidate solution to the problem at hand. The starting population in the MMES evolves toward successively better regions of the search space by means of randomized processes (evolutionary operators), such as recombination, mutation, and selection, until a goal value in the objective function is attained.[11–13] However, in some practical cases, an MMES might stagnate in the local minimum due to the lack of theoretical convergence proof to the near-optimal solution; this phenomenon is sometimes called premature convergence. Recently,[14,15] efforts have been made to address this shortcoming with the aid of the HEOAs.

Therefore, in this hybrid configuration, each resulting individual with the MMES is not included in the next generation directly but used as a seed for the subsequent local search technique (LWLR). The LWLR algorithm searches the neighborhood of each resulting individual and selects a better point to be included in the next generation. Hence, the individuals predicted with the LWLR maintain the necessary diversity to prevent quick convergence to a local minimum, and reliable locating of the near-optimal solution is performed by the use of the evolutionary operators such as those described previously.[16–18]

The numerical results show that the proposed HEOA is robust in real experiments for analyzing interferograms degraded by noise.

The outline of this work is organized as follows. In Sec. 2, we describe the HEOA (MMES-LWLR) in detail. Section 3

*Address all correspondence to: Juan Jaime Sánchez-Escobar, E-mail: jjsanchez@ceti.mx

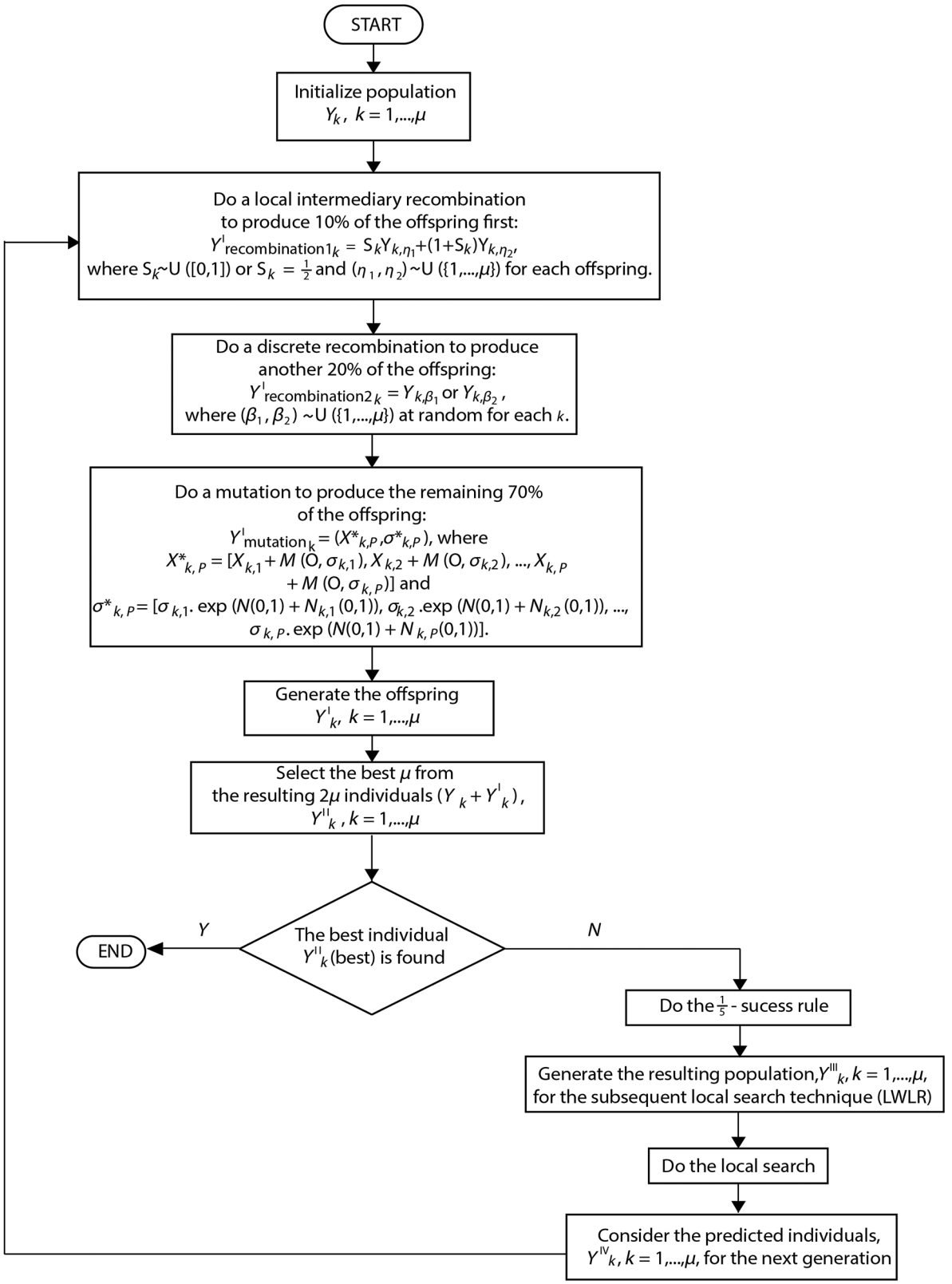

Fig. 1 Flow chart of the hybrid evolutionary optimization algorithm (HEOA).

provides the numerical results and discussions on the solution of the problem for reconstructing the wavefront aberration from a Fizeau interferogram. The conclusions of the paper are summarized in Sec. 4.

2 Proposed Hybrid Evolutionary Optimization Algorithm

The irradiance in the interferogram plane due to the superimposition of two wavefronts is given by Ref. 4.

$$I(x,y) = 2I_0\left[1+\cos\left(\frac{2\pi}{\lambda}\right)w(x,y)\right] + n(x,y), \tag{1}$$

where I_0 specifies that the two waves have equal and uniform intensity, λ is the wavelength of the light, $w(x,y)$ is the unknown wavefront aberration, and $n(x,y)$ represents additive and/or multiplicative noise. Considering that the Zernike polynomials are made up of modes that are of the same form as the types of aberrations observed in optical tests, it is convenient to express the wavefront aberration in polynomial form.[5]

For computing the wavefront aberration from Eq. (1), the inverse problem is reformulated as an optimization problem. Hence, the proposed HEOA minimizes the following objective function based on the Euclidean distance between two interferograms:

$$\mathrm{ED}(I_K, I_{\mathrm{EQ}}) = \sqrt{\sum_{i=1}^{m}\sum_{j=1}^{n}(I_{Ki,j} - I_{\mathrm{EQ}i,j})^2}, \tag{2}$$

where I_{EQ} corresponds to the real interferogram whose intensity histogram has been equalized, while I_K corresponds to the synthetic interferogram optimized in terms of the best individual found $y''_{k(\mathrm{best})}$, $k = 1,\ldots,\mu$, in the i'th iteration or generation. Furthermore, μ represents the number of individuals, which is constant for all generations.

Each individual y''_k in the i'th generation is formed by a real-valued vector that contains elements called object variables $x''_{k,p}$, and each variable is related to a standard deviation, called the strategy parameter $\sigma''_{k,p}$, for carrying on the mutation. Hence, an individual is expressed as follows:[11–13]

$$y''_k = (x''_{k,p}, \sigma''_{k,p}), \qquad p = 1,\ldots,35. \tag{3}$$

In Eq. (3), each object variable represents the p'th Zernike polynomials expansion coefficient. This work considers the list of 35 Zernike polynomials described by Wyant et al., where the modes # 1 through # 35 represent the aberrations to the ninth order.[5] Thus, an individual represents the wavefront aberration necessary to simulate an interferogram I_k.

Since I_K, based on its corresponding y''_k, is simulated considering the pixel values stored in the full range from 0 through 255, the intensity histogram for the experimental interferogram deformed by noise and spatial variations in background/contrast illumination components should be equalized to also cover the full range in order to calculate the Euclidean distance between the two interferograms.[19]

The proposed HEOA takes as an input an equalized experimental interferogram and gives as output the vector of aberration coefficients that best matches it. To do this, the HEOA minimizes Eq. (2) such that $y''_{k(\mathrm{best})}$ satisfies its goal at an acceptable level without being dominated by a local optimum. The flow chart in Fig. 1 describes the procedure followed by our HEOA.

The first step of the HEOA is to create an initial population of parents y_k, $k = 1,\ldots,\mu$, by random selection from a feasible range in each dimension. The distribution of initial trials is typically uniform. Next, the evolutionary operators, such as recombination and mutation, are applied to the set of parents to create a population of offspring y'_k, $k = 1,\ldots,\mu$.

The recombination operator allows information from different individuals of the initial population to be combined, while mutation generates random changes to the rest of the parents.

While the standard configuration in an MMES considers only one recombination operator followed by a mutation operator, in this work the proposed HEOA uses two recombination operators, a local intermediary recombination (LIR) and a discrete recombination (DR), that work as a whole. Hence, the LIR is applied to produce 10% of the offspring first. Next, the DR is applied to produce another 20% of the offspring. Finally, mutation, the main operator, is applied to create the remaining 70% of the offspring.

In the first recombination operator (LIR) described by the HEOA flow chart (again, see Fig. 1), the value of any object variable and strategy parameter in the offspring receives a contribution from a randomly chosen subset of the parents, while in the second recombination operator (DR), the value of each object variable and strategy parameter in an offspring vector comes from one of its parents with equal probability. Also, as can be observed in the HEOA flow chart, the mutation operator generates random changes by adding to each object variable selected $x_{k,p}$ a random variable taken from a normal distribution with mean equal to zero and deviation standard equal to $\sigma_{k,p}$.

The corresponding strategy parameters are mutated by performing the component-wise operation described in Fig. 1, where $N(0,1)$ represents a normally distributed random variable having an expectation of zero and a standard deviation of one, while $N_{k,p}(0,1)$ indicates a random vector, which is sampled again every time the index k changes.

At this point, it is important to remark that the recombination and mutation configuration described earlier in terms of order and the percentage of the initial population they are applied to is the combination in the proposed HEOA that can provide the convergence to the near-optimal solution.

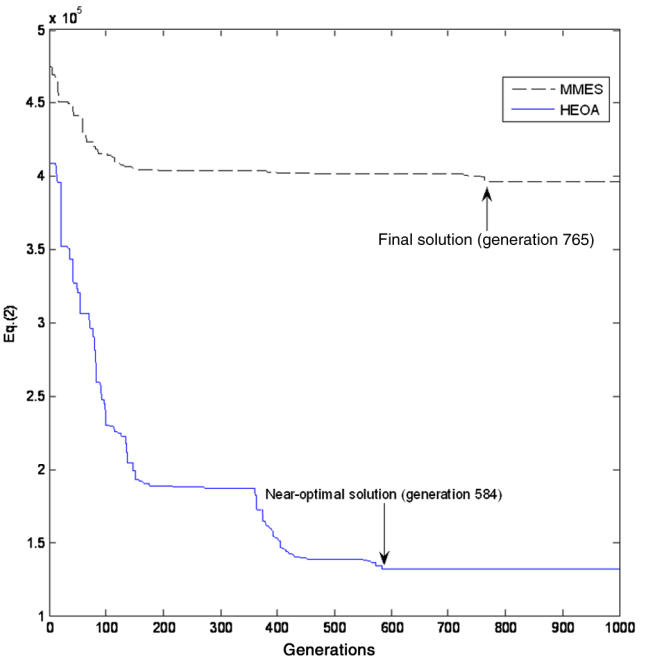

Fig. 2 Behavior described by the multimember evolution strategy (MMES) and the HEOA during the minimization of the objective function specified in Eq. (2).

After the children are obtained, the selection operator chooses the best μ as the parents from the resulting 2μ individuals.

By means of Eq. (2), the fitness value of each individual inside 2μ is calculated. Thus, by ranking the fitness values (errors) y_k and y'_k, $k = 1, \ldots, \mu$, the μ vectors that possess the least error become the new parents.

After selection, a population of new parents is formed, y''_k, $k = 1, \ldots, \mu$; then the strategy parameters $\sigma_{\text{new}_{k,p}}$ of each new parent created from the mutation operator are updated by means of a deterministic adjustment, called the 1/5-success rule, which says that if the estimated probability of successful mutation is $>1/5$, $\sigma_{\text{new}_{k,p}}$ is increased; otherwise, it is decreased, that is, [11–13]

$$\text{If}[\text{fitness}(y''_{\text{mutated}_k}) > \text{fitness}(y_{\text{selected}_k})] > 1/5$$

$$\sigma_{\text{updated}_{k,p}} = \sigma_{\text{new}_{k,p}} * (1 + d), \qquad p = 1, \ldots\ldots, 35.$$

Else

$$\sigma_{\text{updated}_{k,p}} = \sigma_{\text{new}_{k,p}} / d, \qquad p = 1, \ldots\ldots, 35,$$

where d is a small positive constant. For all numerical experiments, we used $d = 0.001$. Furthermore, y_{selected_k} represents the corresponding randomly selected individual from the initial population to be mutated.

Each parent of the resulting population y'''_k, $k = 1, \ldots, \mu$, is not directly entered into the next generation but is used

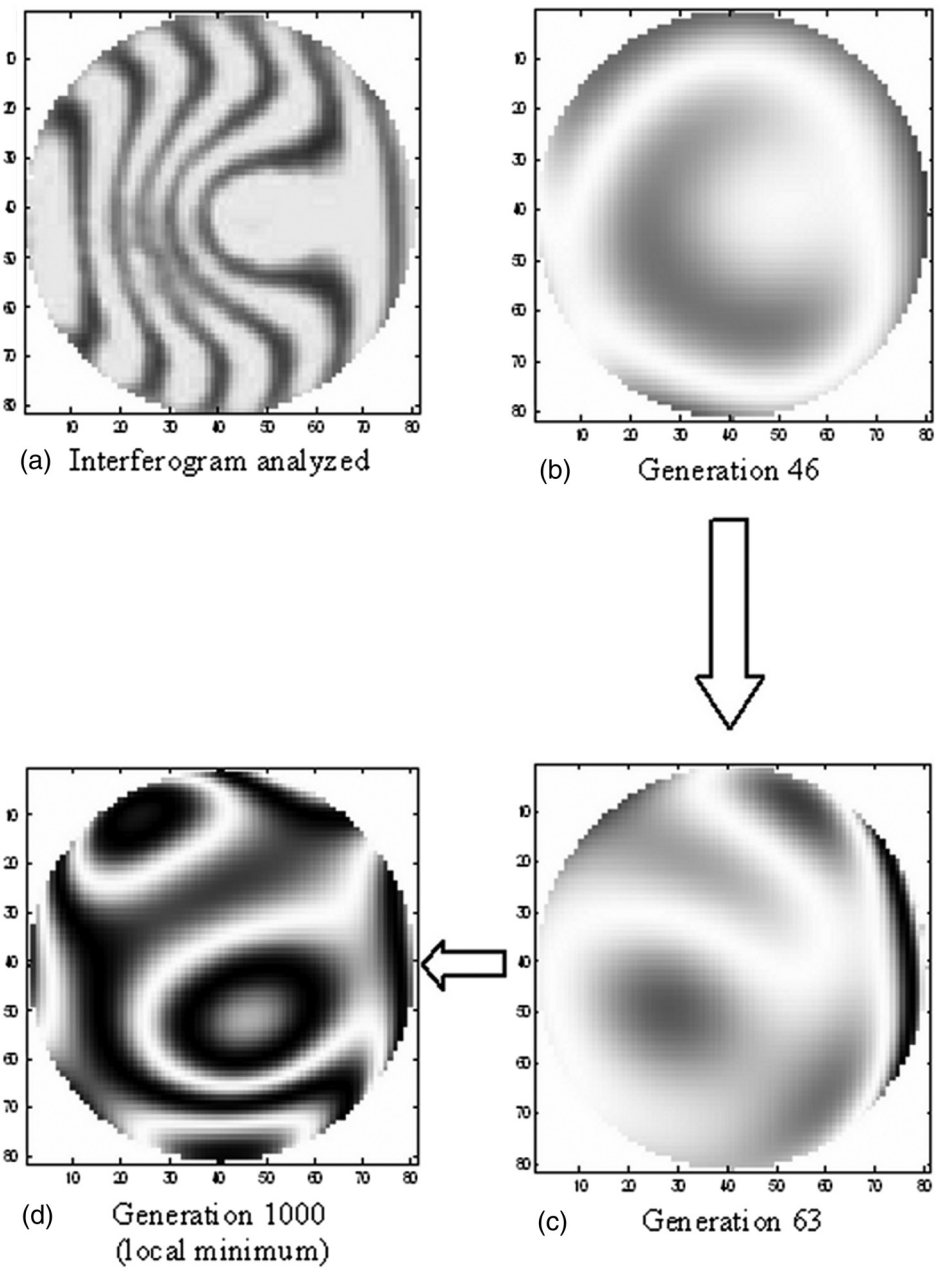

Fig. 3 Interferogram analyzed by the MMES and the synthetic interferograms generated by the best individuals in some generations during the optimization process described in Fig. 2.

as the initial starting point for the subsequent local search technique (LWLR). Hence, each resulting parent y_k''' is used by the LWLR to create a local linear model for predicting another set of individuals,[20,21] y_k^{IV}, $k = 1, \ldots, \mu$, only in a region around the query point (I_{EQ}). Thus, the LWLR algorithm selects a better point in the neighborhood of each resulting parent and generates the next generation, as can be seen in Fig. 1.

The LWLR algorithm starts by assigning a weight w_k for each individual of the resulting population, y_k''', $k = 1, \ldots, \mu$. The weight is calculated by the inverse of the Euclidean distance from I_K, given by the corresponding individual y_k''', to the real interferogram I_{EQ}. Consequently, a diagonal matrix W is created considering diagonal elements $W_{k,k} = w_k$ and zeros elsewhere.

Let X be a matrix whose rows are the vectors of synthetic interferograms generated in terms of the resulting population y_k''', $k = 1, \ldots, \mu$, with the addition of a "1" in the last column. Let Y be a matrix whose rows are the vectors of the resulting population y_k''', $k = 1, \ldots, \mu$. Then the data in X and Y are weighted by means of the following equations:

$$Z = WX, \tag{4}$$

$$V = WY. \tag{5}$$

Then a set of individuals y_k^{IV}, $k = 1, \ldots, \mu$, can be predicted as follows:

$$y_k^{\mathrm{IV}} = I_{\mathrm{EQ}}^T (Z^T Z)^{-1} Z^T V. \tag{6}$$

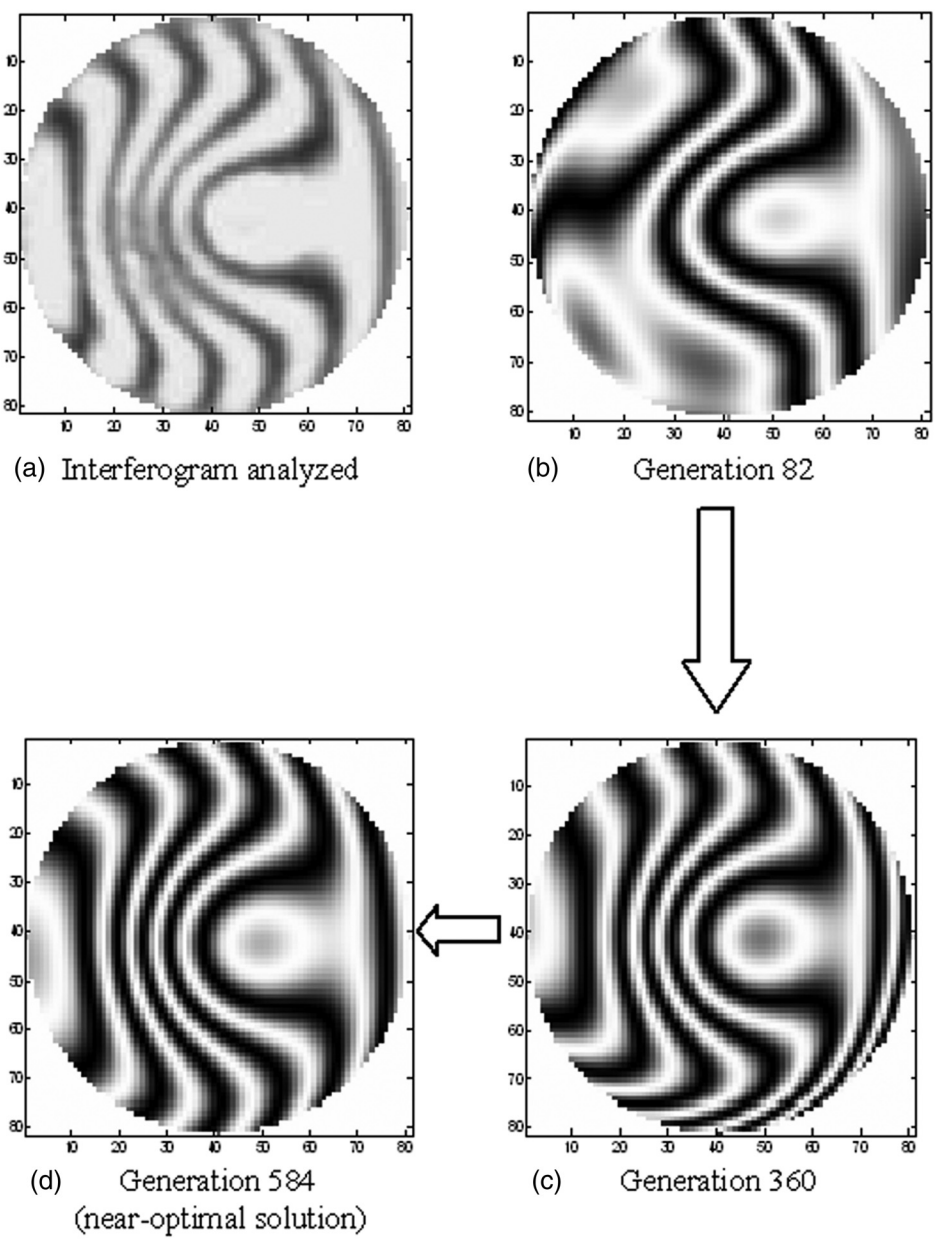

Fig. 4 Interferogram analyzed by the HEOA and the synthetic interferograms generated by the best individuals in different generations during the minimization process shown in Fig. 2.

Table 1 Zernike polynomials expansion coefficients computed by the hybrid evolutionary optimization algorithm (HEOA) in the first part of the numerical study performed.

Mode	Coefficient expressed as multiple of the wavelength used ($\lambda = 632.8$ nm)	Zernike polynomial	Meaning
0	0.4022λ	1	Piston
1	0.1728λ	$\rho \cos\theta$	Tilt *x*
2	-3.1416λ	$\rho \sin\theta$	Tilt *y*
3	0.7663λ	$2\rho^2 - 1$	Focus
4	-0.0411λ	$\rho^2 \cos 2\theta$	Astigmatism *x*
5	-0.0540λ	$\rho^2 \sin 2\theta$	Astigmatism *y*
6	0.2070λ	$(3\rho^2 - 2)\rho \cos\theta$	Coma *x*
7	0.0578λ	$(3\rho^2 - 2)\rho \sin\theta$	Coma *y*
8	-0.7825λ	$6\rho^4 - 6\rho^2 + 1$	Primary spherical
9	-0.0478λ	$\rho^3 \cos 3\theta$	Trefoil *x*
10	0.0062λ	$\rho^3 \sin 3\theta$	Trefoil *y*
11	0.0214λ	$(4\rho^2 - 3)\rho^2 \cos 2\theta$	Secondary astigmatism *x*
12	-0.0195λ	$(4\rho^2 - 3)\rho^2 \sin 2\theta$	Secondary astigmatism *y*
13	-0.1218λ	$(10\rho^4 - 12\rho^2 + 3)\rho \cos\theta$	Secondary coma *x*
14	0.0132λ	$(10\rho^4 - 12\rho^2 + 3)\rho \sin\theta$	Secondary coma *y*
15	0.1677λ	$20\rho^6 - 30\rho^4 + 12\rho^2 - 1$	Secondary spherical
16	0.0000λ	$\rho^4 \cos 4\theta$	Tetrafoil *x*
17	0.0001λ	$\rho^4 \sin 4\theta$	Tetrafoil *y*
18	0.0000λ	$(5\rho^2 - 4)\rho^3 \cos 3\theta$	Secondary trefoil *x*
19	-0.0001λ	$(5\rho^2 - 4)\rho^3 \sin 3\theta$	Secondary trefoil *y*
20	0.0000λ	$(15\rho^4 - 20\rho^2 + 6)\rho^2 \cos 2\theta$	Tertiary astigmatism *x*
21	-0.0000λ	$(15\rho^4 - 20\rho^2 + 6)\rho^2 \sin 2\theta$	Tertiary astigmatism *y*
22	0.0000λ	$(35\rho^6 - 60\rho^4 + 30\rho^2 - 4)\rho \cos\theta$	Tertiary coma *x*
23	0.0000λ	$(35\rho^6 - 60\rho^4 + 30\rho^2 - 4)\rho \sin\theta$	Tertiary coma *y*
24	-0.0000λ	$70\rho^8 - 140\rho^6 + 90\rho^4 - 20\rho^2 + 1$	Tertiary spherical
25	-0.0000λ	$\rho^5 \cos 5\theta$	Pentafoil *x*
26	0.0000λ	$\rho^5 \sin 5\theta$	Pentafoil *y*
27	0.0001λ	$(6\rho^2 - 5)\rho^4 \cos 4\theta$	Secondary tetrafoil *x*
28	0.0000λ	$(6\rho^2 - 5)\rho^4 \sin 4\theta$	Secondary tetrafoil *y*
29	0.0000λ	$(21\rho^4 - 30\rho^2 + 10)\rho^3 \cos 3\theta$	Tertiary trefoil *x*
30	-0.0000λ	$(21\rho^4 - 30\rho^2 + 10)\rho^3 \sin 3\theta$	Tertiary trefoil *y*
31	-0.0000λ	$(56\rho^6 - 105\rho^4 + 60\rho^2 - 10)\rho^2 \cos 2\theta$	Quaternary astigmatism *x*
32	-0.0000λ	$(56\rho^6 - 105\rho^4 + 60\rho^2 - 10)\rho^2 \sin 2\theta$	Quaternary astigmatism *y*
33	0.0000λ	$(126\rho^8 - 280\rho^6 + 210\rho^4 + 60\rho^2 + 5)\rho \cos\theta$	Quaternary coma *x*
34	-0.0000λ	$(126\rho^8 - 280\rho^6 + 210\rho^4 + 60\rho^2 + 5)\rho \sin\theta$	Quaternary coma *y*
35	-0.0000λ	$252\rho^{10} - 630\rho^8 + 560\rho^6 - 210\rho^4 + 30\rho^2 - 1$	Quaternary spherical

3 Numerical Results

In the first part of the numerical study conducted, Fig. 2 shows the minimization procedure described by MMES when the fitness of the best individual in terms of Eq. (2) is plotted against the generation number (dashed black line).

When the initial population is randomly generated and each individual is formed by a considerable number of Zernike polynomials expansion coefficients (35 coefficients in the present optimization problem), the MMES cannot prevent premature convergence to a local minimum, as can be observed in Fig. 2. This occurs due to the lack of population diversity.

It can be seen in Fig. 2 that the local minimum produced by MMES as the final solution to the optimization problem is found without any change after about 764 generations. Consequently, the similarity between the interferogram retrieved as the final solution and the analyzed Fizeau interferogram is very poor [see Figs. 3(a) and 3(d), respectively]. In Fig. 3, each synthetic interferogram I_k corresponds to the best individual of its generation within the optimization process shown in Fig. 2.

If additional information about the solution of the optimization problem is available as proportioned by a local search technique (LWLR), then such information should be considered as the current population in the next iteration, which can prevent local optima from being generated within the MMES. Once such additional information is used by the MMES, it can be successfully applied to solve Eq. (2), avoiding a premature convergence to a local minimum.

Also shown in Fig. 2 as a solid blue line is the behavior described by the proposed HEOA in order to minimize the objective function in Eq. (2) avoiding local minima. As can be noted, the near-optimal solution is obtained by the HEOA after 583 generations. Figure 4 shows the Fizeau interferogram under analysis, which corresponds to the same interferogram analyzed by MMES, and the interferograms already generated by the fittest individuals in some generations during the optimization process described by HEOA.

In Fig. 2, most of the progress given by HEOA occurs early in the search due to the end of the flat curve in generation 360, and the synthetic interferogram generated by the best individual in this generation [see Fig. 4(c)] already tends to be similar to the Fizeau interferogram, although not enough compared to the interferogram obtained in the last generation [Fig. 4(d)], which is practically identical to the Fizeau interferogram. Sometimes the HEOA describes a flat curve, as shown in Fig. 2 from generation 164 to 360, even when the algorithm usually converges to the near-optimal solution between the 500th and 600th generations.

Considering the near-optimal solution found in the first part of our numerical study, we assume that the HEOA shows validity in reconstructing, from the Fizeau interferogram, the wavefront aberration in terms of their Zernike polynomial coefficients computed to the fifth order once the objective function that depends on the Euclidean distance has been minimized while avoiding a local minimum. In Table 1, it can be observed that the significant contribution to the wavefront aberration reconstructed by the HEOA is contained in the first 15 modes, while the contribution of the remaining modes is not meaningful compared with those of the first 15 modes.

Figure 5 shows the three-dimensional (3-D) plot of the wavefront aberration reconstructed from the first Fizeau interferogram by considering the Zernike polynomial expansion coefficients shown in Table 1. In Fig. 5, the wavefront aberration is shown by removing the pseudoaberrations, such as piston, tilt x, tilt y, and focus.

The second part of the numerical study aims to test the performance of the HEOA in computing, from a second real interferogram, the Zernike polynomial coefficients to the third order, discarding the higher-order Zernike polynomial expansion coefficients during the optimization process. To do this, we have selected a Fizeau interferogram whose OPD can be expressed in terms of third-order aberrations.

Figure 6 shows the performance of HEOA, a second Fizeau interferogram to be analyzed, and the synthetic interferograms generated by the fittest individuals at some generations during the optimization process. As can be observed, the similarity between the interferogram retrieved as the near-optimal solution in generation 513 and the analyzed real interferogram is very good. This numerical result makes it clear that the HEOA is also capable of reconstructing the wavefront aberration from the second Fizeau interferogram. Thus, the ability of the HEOA to solve Eq. (2) is similar to that obtained in the first part of the numerical study. The Zernike polynomial coefficients calculated in the second part of the numerical study are shown in Table 2.

According to the numerical results shown in Table 2, the wavefront aberration reconstructed by the HEOA during the second part of the numerical study is then defined by third-order aberrations, such as piston, tilt x, tilt y, focus, astigmatism x, astigmatism y, coma x, coma y, and primary spherical aberration, while the remaining Zernike polynomial expansion coefficients tend to be equal to zero.

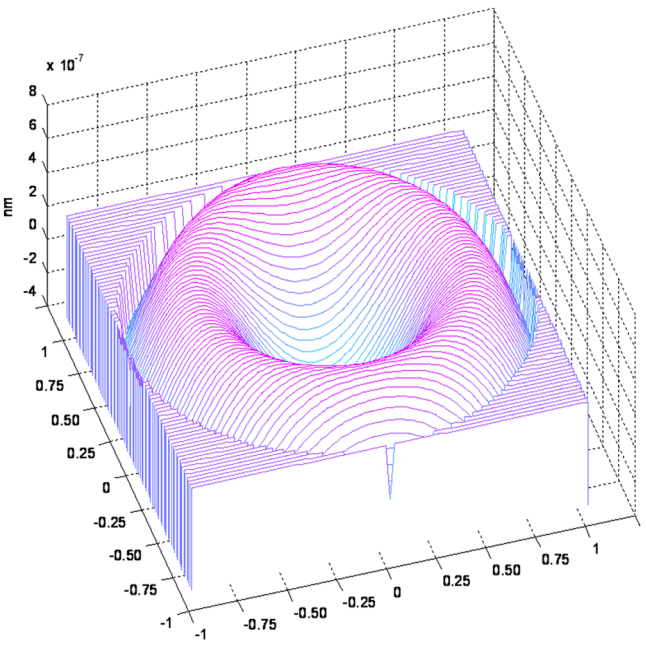

Fig. 5 Three-dimensional (3-D) plot of the wavefront aberration reconstructed from the first Fizeau interferogram by the use of HEOA. The wavefront aberration is shown by removing the pseudo aberrations, such as piston, tilt x, tilt y, and focus.

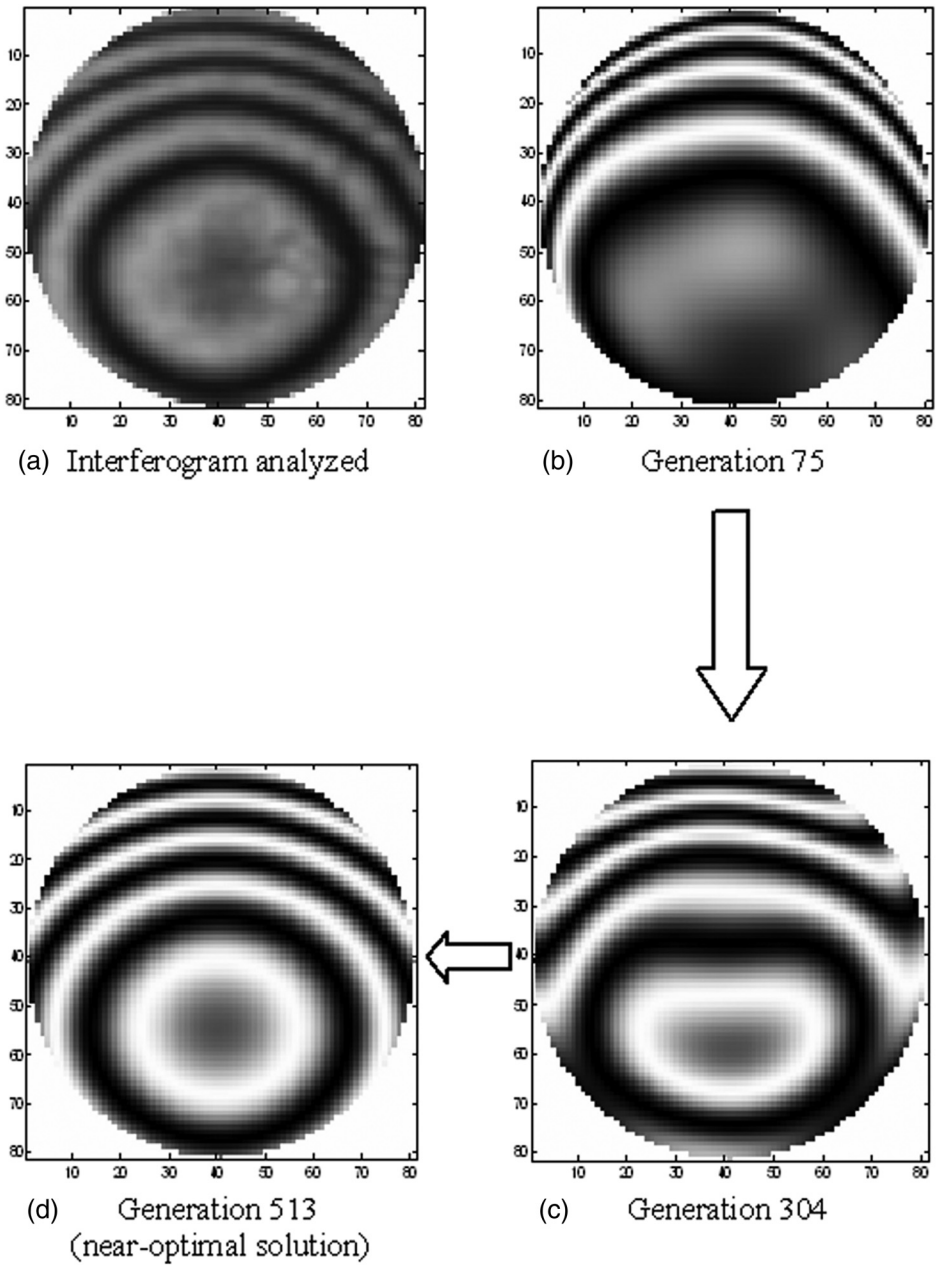

Fig. 6 Second interferogram analyzed and the synthetic interferograms generated by the fittest individuals in different generations within the optimization process performed by HEOA. The near-optimal solution is obtained after 512 generations.

Figure 7 shows the 3-D plot of the wavefront aberration reconstructed from the second Fizeau interferogram by considering the Zernike polynomial expansion coefficients shown in Table 2. Also, in Fig. 7, the wavefront aberration is shown with the pseudoaberrations removed.

It is important to mention that even though both Fizeau interferograms are equalized, it is evident that the first interferogram is analyzed containing a broken fringe, as shown in Fig. 8, while the second real interferogram is analyzed containing a distortion caused by the diffraction of dust particles in the optical paths, as indicated in Fig. 9. However, the HEOA has proven to be robust in both numerical studies.

In all of the numerical experiments, we used a personal computer equipped with a 2.80 GHz Pentium-4 processor and we chose the software MATLAB™ since it allows a program to be written in the simplest form. The numerical experiments performed by the HEOA took about 251 s using a population size equal to 50. Hence, a program implemented in MATLAB programming language is slow because the operations must be interpreted before being performed. However, an efficient code can be generated from a MATLAB™ program by using a translator. A study related to this alternative is not intended to form part of this paper.

Finally, it is important to remark that the number of Zernike modes used by the HEOA for the reconstruction of the wavefront aberration in the second part of the numerical study is similar to that obtained with the covariance matrix method recently proposed by Yu et al., to analyze the wavefront aberrations for the circle interference fringe of a fine polished aluminum disk surface captured by a

Table 2 Zernike polynomials expansion coefficients computed by HEOA in the second part of the numerical study performed.

Mode	Coefficient expressed as multiple of the wavelength used ($\lambda = 632.8$ nm)	Zernike polynomial
0	1.0324λ	1
1	-1.6467λ	$\rho\cos\theta$
2	0.0248λ	$\rho\sin\theta$
3	1.0364λ	$2\rho^2-1$
4	-0.3207λ	$\rho^2\cos 2\theta$
5	-0.0034λ	$\rho^2\sin 2\theta$
6	0.0027λ	$(3\rho^2-2)\rho\cos\theta$
7	-0.0078λ	$(3\rho^2-2)\rho\sin\theta$
8	-0.0040λ	$6\rho^4-6\rho^2+1$
9	0.0001λ	$\rho^3\cos 3\theta$
10	0.0000λ	$\rho^3\sin 3\theta$
11	0.0001λ	$(4\rho^2-3)\rho^2\cos 2\theta$
12	0.0000λ	$(4\rho^2-3)\rho^2\sin 2\theta$
13	0.0000λ	$(10\rho^4-12\rho^2+3)\rho\cos\theta$
14	-0.0000λ	$(10\rho^4-12\rho^2+3)\rho\sin\theta$
15	0.0000λ	$20\rho^6-30\rho^4+12\rho^2-1$
16	0.0000λ	$\rho^4\cos 4\theta$
17	0.0000λ	$\rho^4\sin 4\theta$
18	0.0000λ	$(5\rho^2-4)\rho^3\cos 3\theta$
19	0.0000λ	$(5\rho^2-4)\rho^3\sin 3\theta$
20	0.0000λ	$(15\rho^4-20\rho^2+6)\rho^2\cos 2\theta$
21	0.0000λ	$(15\rho^4-20\rho^2+6)\rho^2\sin 2\theta$
22	0.0000λ	$(35\rho^6-60\rho^4+30\rho^2-4)\rho\cos\theta$
23	0.0000λ	$(35\rho^6-60\rho^4+30\rho^2-4)\rho\sin\theta$
24	-0.0000λ	$70\rho^8-140\rho^6+90\rho^4-20\rho^2+1$
25	-0.0000λ	$\rho^5\cos 5\theta$
26	0.0000λ	$\rho^5\sin 5\theta$
27	-0.0000λ	$(6\rho^2-5)\rho^4\cos 4\theta$
28	0.0000λ	$(6\rho^2-5)\rho^4\sin 4\theta$
29	0.0000λ	$(21\rho^4-30\rho^2+10)\rho^3\cos 3\theta$
30	0.0000λ	$(21\rho^4-30\rho^2+10)\rho^3\sin 3\theta$
31	0.0000λ	$(56\rho^6-105\rho^4+60\rho^2-10)\rho^2\cos 2\theta$
32	0.0000λ	$(56\rho^6-105\rho^4+60\rho^2-10)\rho^2\sin 2\theta$
33	0.0000λ	$(126\rho^8-280\rho^6+210\rho^4+60\rho^2+5)\rho\cos\theta$
34	0.0000λ	$(126\rho^8-280\rho^6+210\rho^4+60\rho^2+5)\rho\sin\theta$
35	0.0000λ	$252\rho^{10}-630\rho^8+560\rho^6-210\rho^4+30\rho^2-1$

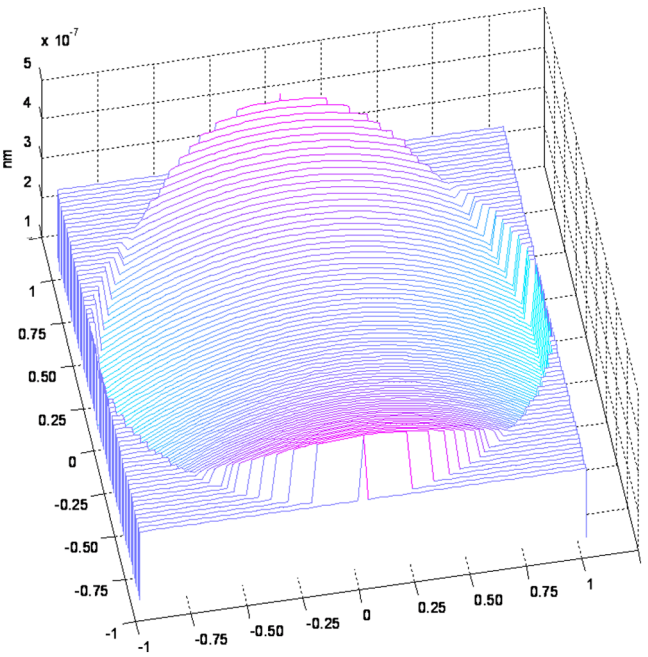

Fig. 7 3-D plot of the wavefront aberration reconstructed from the second Fizeau interferogram by the use of HEOA. The wavefront aberration is shown by removing the pseudoaberrations, such as piston, tilt x, tilt y, and focus.

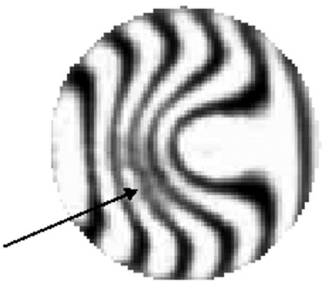

Fig. 8 First interferogram analyzed. The arrow indicates a broken fringe.

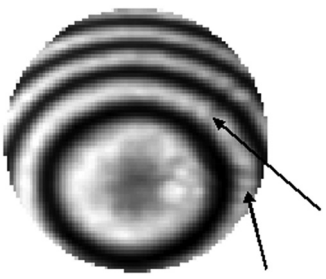

Fig. 9 Second interferogram analyzed. The arrows indicate a distortion caused by the diffraction of dust particles in the optical paths.

Twyman-Green interferometer system.[9] In that work, 35-mode Zernike coefficients are provided to express the wavefront aberrations and an experimental interpretation of the Zernike coefficients' stability is given. Hence, considering each wavefront aberration reconstructed with the different Zernike modes from 10 to 35, we noted that the covariance matrix method maintains not only higher fitting precision,

but also the correct expression for the wavefront aberration when the number of Zernike modes is 10.

4 Conclusions

This paper has presented a study of the performance of HEOA based on the combination of MMES and LWLR for reconstructing the wavefront aberration from a real interferogram by the use of Zernike polynomials.

The numerical results proved that HEOA has the ability not only to calculate the correct values of the Zernike polynomial expansion coefficients, but also to find the correct number of Zernike modes even when each Fizeau interferogram is degraded by noise (see Figs. 8 and 9).

It is important to note that the pseudoaberration search space in HEOA is restricted in each numerical trial to preserve the numerical stability. Thus, the reconstruction of the wavefront aberrations is carried out by considering a reduced number of fringes. However, the proposed algorithm could be applied to corroborate with precision the quality of a manufactured optical surface once the tilt and defocusing have been reduced in the Fizeau interferometer system.

Acknowledgment

We thank the SUTCETI and Dirección General-CETI for the support given to the completion of this work.

References

1. D. Malacara, *Optical Shop Testing*, J. Wiley and Sons, Hoboken (2007).
2. D. Malacara, M. Servin, and Z. Malacara, *Interferogram Analysis for Optical Testing*, CRC Press, Boca Raton (2005).
3. I. K. Sung et al., "A swing arm method for profile measurement of large optical concave surfaces in the lapping process," *Int. J. Adv. Manuf. Technol.* **29**, 113–117 (2006).
4. J. J. Briers, "Optical testing: a review and tutorial for optical engineers," *Opt. Lasers Eng.* **32**, 111–138 (1999).
5. J. C. Wyant and K. Creath, "Basic wavefront aberration theory for optical metrology," Chapter 1 in *Applied Optics and Optical Engineering*, R. R. Shannon, J. C. Wyant, and W. Corporation, Eds., pp. 1–53, Academic Press, Inc., San Diego, California (1992).
6. D. Malacara, J. M. Carpio, and J. J. Sánchez, "Wavefront fitting with discrete orthogonal polynomials in a unit radius circle," *Opt. Eng.* **29**(6), 672–675 (1990).
7. J. Y. Wang and D. E. Silva, "Wave-front interpolation with Zernike polynomials," *Appl. Opt.* **19**(9), 1510–1518 (1980).
8. D. R. Iskander, M. J. Collins, and B. Davis, "Optimal modeling of corneal surfaces with Zernike polynomials," *IEEE Trans. Biomed. Eng.* **48**(1), 87–95 (2001).
9. X. Yu et al., "Stability of Zernike coefficients solved by the covariance matrix method in the analysis of the wave front aberration," *Optik* **122**, 1701–1706 (2011).
10. X. Yu et al., "The influence of the sampling dots on the analysis of the wave front aberration by using the covariance matrix method," *Optik* **123**, 792–795 (2012).
11. T. Bäck, F. Hoffmeister, and H. P. Schwefel, "A survey of evolution strategies," http://bi.snu.ac.kr/Info/EC/A%20Survey%20of%20Evolution%20Strategies.pdf
12. T. Bäck, *Evolutionary Algorithms in Theory and Practice*, Oxford University Press, New York (1996).
13. D. B. Foggel, *Evolutionary Computation*, IEEE Press, New York (2000).
14. A. Lara et al., "HCS: a new local search strategy for memetic multiobjective evolutionary algorithms," *IEEE Trans. Evol. Comput.* **14**(1), 112–132 (2010).
15. K. Sindhya, K. Miettinen, and K. Deb, "A hybrid framework for evolutionary multi-objective optimization," *IEEE Trans. Evol. Comput.* **17**(4), 495–511 (2013).
16. K. Sindhya, K. Deb, and K. Miettinen, "Improving convergence of evolutionary multi-objective optimization with local search: a concurrent-hybrid algorithm," *Nat. Comput.* **10**(4), 1407–1430 (2011).
17. K. Sindhya, K. Miettinen, and K. Deb, "An improved concurrent-hybrid algorithm for enhanced diversity and accuracy in evolutionary multi-objective optimization," in *Evolutionary and Deterministic Methods for Design, Optimization and Control, Applications to Industrial and Societal Problems*, T. Burczynski and J. Periaux, Eds., pp. 182–187, CINME, Barcelona, Spain (2011).
18. H. Ishibuchi et al., "How to choose solutions for local search in multiobjective combinatorial memetic algorithms," *Lec. Notes Comput. Sci.* **6238**, 516–525 (2010).
19. J. C. Russ, *The Image Processing Handbook*, CRC Press, Boca Raton (2011).
20. T. M. Mitchell, *Machine Learning*, McGraw-Hill, Boston (1997).
21. C. G. Atkenson, A. W. Moore, and S. Schaal, "Locally weighted learning," *Artif. Intell. Rev.* **11**, 11–73 (1997).

Juan Jaime Sánchez Escobar received his Bachelor of Engineering degree in electronics from the Tuxtla Gutiérrez Technological Institute, Chiapas, México, and his PhD from the National Institute of Astrophysics, Optics, and Electronic, México. He has been with the research department at the Center for Industrial and Technical Teaching since 2003. His research interests include techniques for 2D phase unwrapping and phase retrieval as applied to 3D machine vision and machine learning applications.

Liliana Ibeth Barbosa Santillán is currently the junior researcher at UDG University in Guadalajara, México. She received her BS degree in computer science from Puebla Autonomous University. She has a MS degree in computer science from the National Institute of Astrophysics, Optics and Electronics and her DEA in computer science at the Technical University of Madrid, Spain. She is a PhD candidate in applied mathematics from the Department of Computer Sciences at Technical University of Madrid, Spain.